Mechanism for OO bond formation in a biomimetic tetranuclear manganese cluster – A density functional theory study

ARTICLE *in* JOURNAL OF PHOTOCHEMISTRY AND PHOTOBIOLOGY B BIOLOGY · DECEMBER 2014

Impact Factor: 2.96 · DOI: 10.1016/j.jphotobiol.2014.12.005 · Source: PubMed

Journal of Photochemistry and Photobiology B: Biology xxx (2014) xxx–xxx

Contents lists available at ScienceDirect

Journal of Photochemistry and Photobiology B: Biology

journal homepage: www.elsevier.com/locate/jphotobiol

Mechanism for O—O bond formation in a biomimetic tetranuclear manganese cluster – A density functional theory study

Rong-Zhen Liao *, Per E.M. Siegbahn *

Department of Organic Chemistry, Arrhenius Laboratory, Stockholm University, SE-10691 Stockholm, Sweden

ARTICLE INFO

Article history:
Received 28 October 2014
Received in revised form 25 November 2014
Accepted 1 December 2014
Available online xxxx

ABSTRACT

Density functional theory calculations have been used to study the reaction mechanism of water oxidation catalyzed by a tetranuclear Mn-oxo cluster $Mn_4O_4L_6$ ($L = (C_6H_4)_2PO_4^-$). It is proposed that the O—O bond formation mechanism is different in the gas phase and in a water solution. In the gas phase, upon phosphate ligand dissociation triggered by light absorption, the O—O bond formation starting with both the Mn_4(III,III,IV,IV) and Mn_4(III,IV,IV,IV) oxidation states has to take place via direct coupling of two bridging oxo groups. The calculated barriers are 42.3 and 37.1 kcal/mol, respectively, and there is an endergonicity of more than 10 kcal/mol. Additional photons are needed to overcome these large barriers. In water solution, water binding to the two vacant sites of the Mn ions, again after phosphate dissociation triggered by light absorption, is thermodynamically and kinetically very favorable. The catalytic cycle is suggested to start from the Mn_4(III,III,III,IV) oxidation state. The removal of three electrons and three protons leads to the formation of a Mn_4(III,IV,IV,IV)-oxyl radical complex. The O—O bond formation then proceeds via a nucleophilic attack of water on the Mn^{IV}-oxyl radical assisted by a Mn-bound hydroxide that abstracts a proton during the attack. This step was calculated to be rate-limiting with a total barrier of 29.2 kcal/mol. This is followed by proton-coupled electron transfer, O_2 release, and water binding to start the next catalytic cycle.

1. Introduction

The development and production of clean and sustainable fuels is one of the most challenging tasks facing scientists in this century. One attractive solution would be to design artificial leaves that utilize solar energy to split water into O_2 and H_2. About 3 billion years ago, nature developed a delicate photosynthetic system that can capture sunlight and convert it into chemical energy to oxidize water into O_2 and to reduce CO_2 into biomass [1–4]. In this process, the oxidation of water is catalyzed by the Mn_4Ca cluster in the oxygen evolving complex (OEC) of photosystem II (PSII). Considerable efforts have been dedicated to the synthesis of Mn-based multinuclear complexes that mimic the structure and function of OEC [5–14].

Dismukes and co-workers have reported the synthesis of a series of tetranuclear Mn-oxo cluster [15–28], $Mn_4O_4L_6$ ($L = (p\text{-R-}C_6H_4)_2PO_4^-$, R = H, CH_3, OCH_3), which catalyzes photochemical water oxidation utilizing a TiO_2-supported $[Ru^{II}(bipy)_2(bipy(COO)_2)]$-type photosensitizer. They investigated the process both in water solution [28] and in gas phase [18,19]. In the catalytic process in water, the Mn_4 cluster was immobilized on a Nafion membrane-coated conductive electrode and immersed in an aqueous solution (pH = 6.5). Kinetic investigations showed a turnover number (TON; defined as moles of O_2 produced per mole catalyst) of more than 1000 and a turnover frequency (TOF; defined as moles of O_2 produced per mole catalyst per unit time) of 47 h^{-1}, which can be translated into a barrier of about 20 kcal/mol, using classical transition state theory. Upon light excitation, the Ru^{II} dye donates one electron to the TiO_2 band and a one-electron oxidant $[Ru^{III}(bipy)_2(bipy(COO)_2)]^+$ is generated with a reduction potential of 1.4 V. This Ru^{III} complex is capable of oxidizing the Mn_4 cluster from Mn_4(II,II,III,III) (**1**) to Mn_4(III,III,IV,IV) (**5**) via four sequential proton-coupled electron transfer (PCET) steps (Scheme 1) [25]. From **5**, the O—O bond formation takes place upon excitation by a second beam of light [28]. Very importantly, the excitation process involves the dissociation of one phosphate ligand to generate **6**, which was found to be required for the O—O bond formation [18].

In gas phase, photo-excitation of **5** at 337 nm (Mn—O charge transfer excitation) followed by a laser desorption/ionization mass spectrometry (LDI-MS) analysis showed that the formation of O_2 is associated with the dissociation of one phosphate ligand [18]. Further an ^{18}O isotope labeling study confirmed that both oxygen atoms in O_2 came from the parent complex **5** [19]. When only *d–d* ligand field excitation (532 nm) was involved, no product

* Tel.: +46 162616.
E-mail addresses: rongzhen@organ.su.se (R.-Z. Liao), ps@organ.su.se (P.E.M. Siegbahn).

http://dx.doi.org/10.1016/j.jphotobiol.2014.12.005
1011-1344/

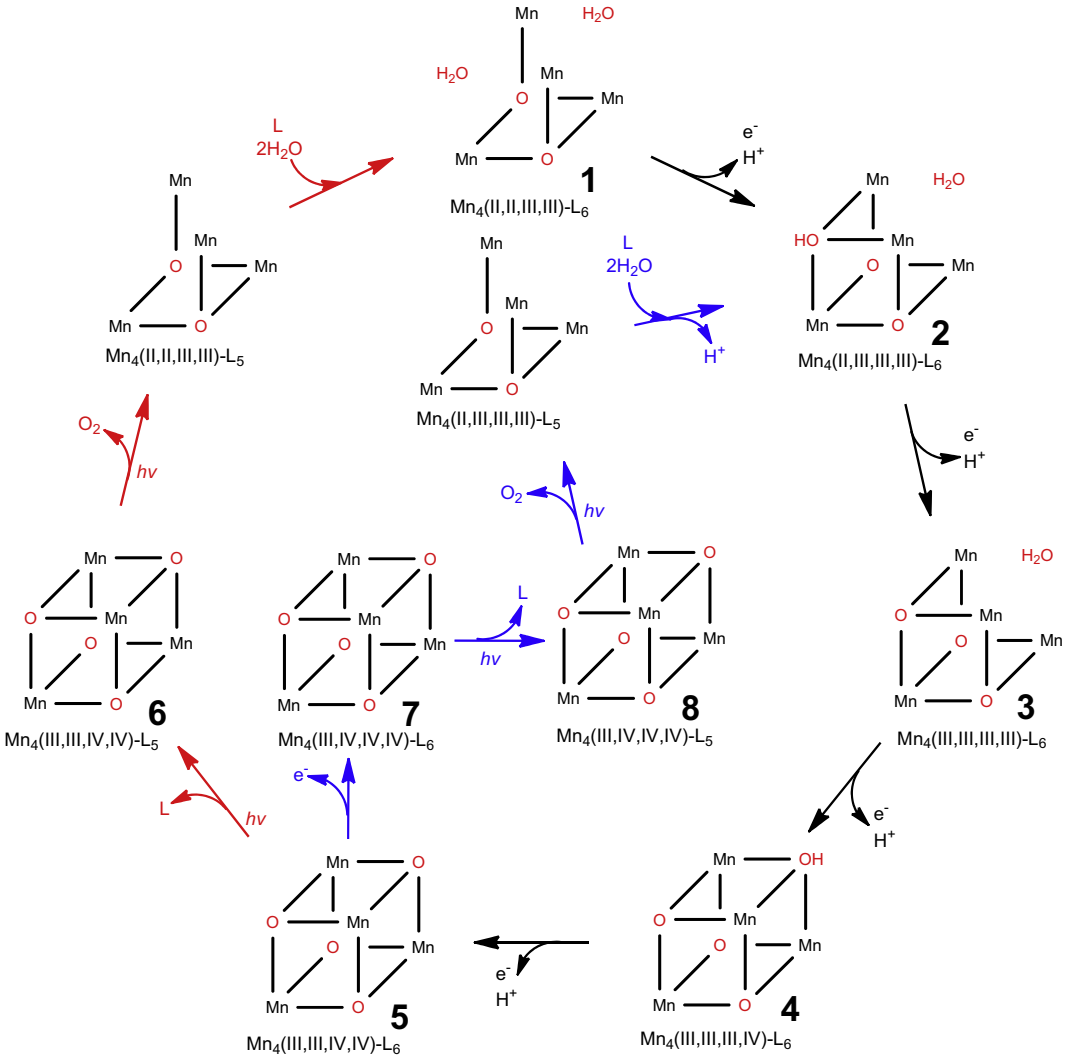

Scheme 1. Proposed photocatalytic cycle of water oxidation catalyzed by the Dismukes Mn_4 complex [25].

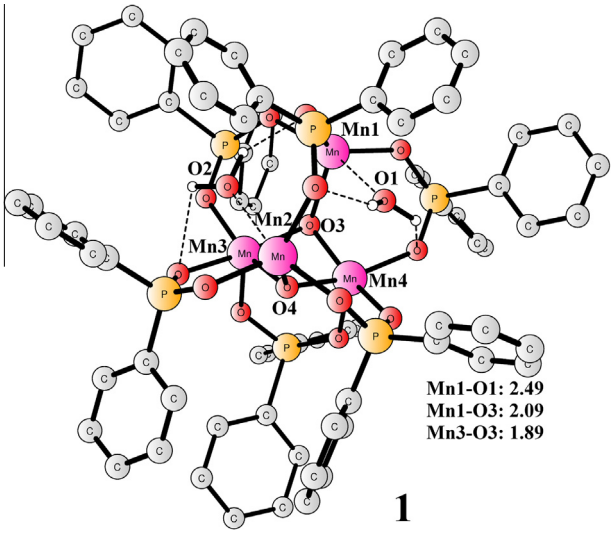

Fig. 1. Optimized structure of **1**(Mn_4(II,II,III,III)). Distances are given in Angstrom. For clarity, hydrogen atoms on phenyl rings are not shown.

Table 1
Spin density on Mn and Mn–Mn distances (in Angstrom) of structures **1–8**.

	1	2	3	4	5	6	7	8	5(exp)	7(exp)
Spin density										
Mn1	4.83	3.96	3.95	3.93	3.91	3.89	3.89	3.89	–	–
Mn2	4.83	4.84	3.95	3.93	3.91	3.89	3.04	3.89		
Mn3	3.97	3.94	3.94	3.93	3.11	3.06	3.05	3.06		
Mn4	3.97	3.94	3.93	3.14	3.10	3.06	3.05	3.06		
Distances										
Mn1–Mn2	4.24	3.48	3.20	3.18	3.12	2.93	2.91	2.92	2.9826	2.904
Mn1–Mn3	3.46	3.19	3.10	3.17	2.84	2.91	3.02	2.91	2.9038	~
Mn1–Mn4	3.29	3.08	3.01	2.92	3.03	2.91	3.01	2.92	2.9126	2.954
Mn2–Mn3	3.29	3.42	3.18	3.17	3.03	2.90	2.86	2.92	2.8341	
Mn2–Mn4	3.46	3.31	2.88	2.91	2.86	2.90	2.86	2.91	2.8377	
Mn3–Mn4	2.81	2.84	3.00	2.93	2.83	2.80	2.81	2.79	2.8588	

could be detected [19]. It was shown that **5** can undergo one electron oxidation to generate Mn_4(III,IV,IV,IV) (**7**), in which ligand dissociation can form **8** and then release O_2 with a similar mechanism as **6** [24].

The mechanism of the O—O bond formation in Mn_4(III,III,IV,IV)-L_5 has previously been investigated using density functional calcu-

Please cite this article in press as: R.-Z. Liao, P.E.M. Siegbahn, Mechanism for O—O bond formation in a biomimetic tetranuclear manganese cluster – A density functional theory study, J. Photochem. Photobiol. B: Biol. (2014), http://dx.doi.org/10.1016/j.jphotobiol.2014.12.005

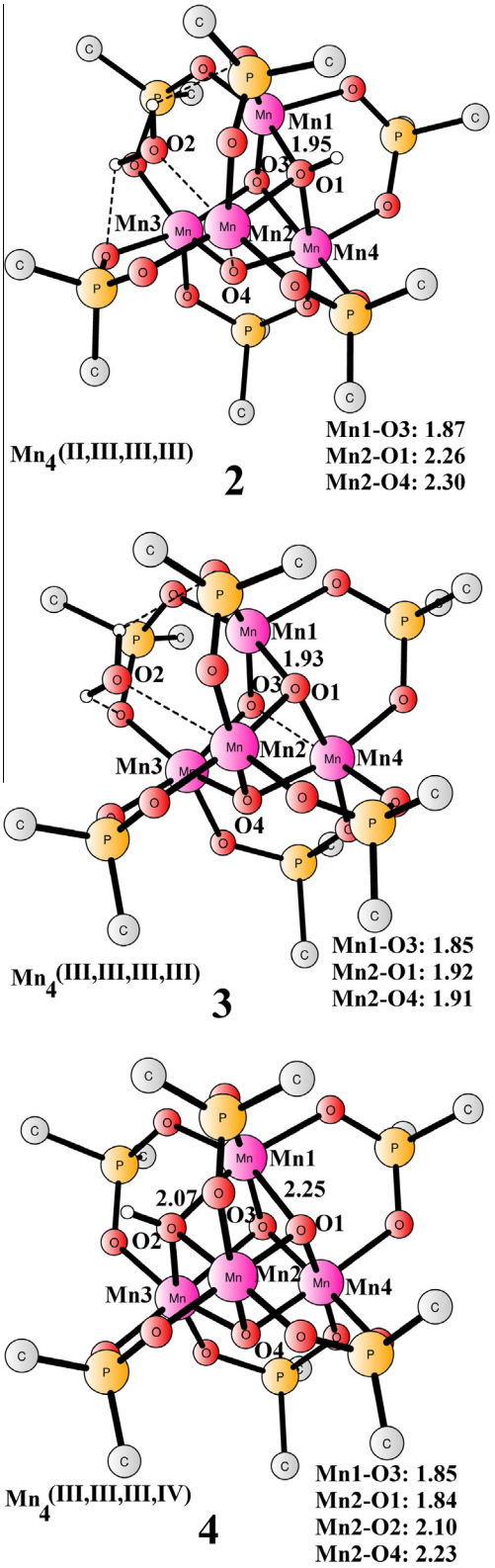

Fig. 2. Optimized structures of **2**, **3**, and **4**. Distances are given in Angstrom. For clarity, the phenyl rings are represented by carbon atoms. For full model, see Fig. 1.

lations using a small model, in which the phenyl groups of $Ph_2PO_2^-$ were represented by hydrogens [29]. It was shown that the direct coupling of the two bridging oxo groups had a barrier of 28.3 kcal/mol in the gas phase, and this barrier increased to 33.4 kcal/mol when water solvation effects were included. This step was found to be rate-limiting, and the following O_2 release was very facile.

In the present study, we report density functional calculations on the reaction mechanism of water oxidation catalyzed by this tetranuclear Mn cubane cluster using a full model of the complex. The structures of various redox intermediates and the redox potentials of redox couples were calculated and analyzed. The O—O bond formation mechanism in the gas phase and in a water solution was studied by adding three explicit water molecules. A full energy diagram of the catalytic cycle in water solution was constructed using a similar methodology as used in our previous studies on PSII and other artificial water oxidation catalysts [30–37].

2. Computational details

The geometry optimizations in the present study were performed using the density functional B3LYP [38] as implemented in the Gaussian 09 [39] program. The 6-31G(d,p) basis set was used for the C, O, P, H elements and the SDD pseudopotential [40] for Mn. On the basis of these optimized geometries, single-point calculations were performed to obtain more accurate energies employing a larger basis set 6-311 + G(2d,2p) for all elements except Mn at the B3LYP* (15% exact exchange) [41] level. Recent comparisons of the performance of different density functionals on the energy diagram of water oxidation by PSII suggested that B3LYP* gave the most reliable results compared with experimental data [35]. The water solvation effects were calculated using the SMD [42] continuum solvation model with the larger basis set at the B3LYP* level. For water, the experimental solvation free energy of −6.3 kcal/mol is used [43]. All stationary points were confirmed as minima or transition states by analytic frequency calculations at the same level of theory as the geometry optimizations. D2 dispersion corrections proposed by Grimme [44] were also added in single-point calculations. The concentration correction of 1.9 kcal/mol at room temperature (derived from the free-energy change of 1 mol of an ideal gas from 1 atm (24.5 L/mol, 298.15 K) to 1 M) were added for all species except water, for which 4.3 kcal/mol is used as the standard state of the water solvent is 55.6 M. The values reported here are the B3LYP*-D2 energies, including Gibbs free energy corrections and D2 dispersion from B3LYP.

To calculate the redox potentials of various redox couples, the experimental driving force ($4 \cdot (0.846–1.40) \cdot 23.06 = -51.1$ kcal/mol) derived from the over-potential (1.40 V for Ru^{III}/Ru^{II}, and 0.846 V for water oxidation at pH = 6.5) [28] was used to set up the reference energy for PCET, which is 408.6 kcal/mol for the release of (H^+, e^-). To calculate p*K*a, the gas phase free energy of a proton (−6.3 kcal/mol) and the experimental solvation free energy of a proton (−264.0 kcal/mol) [43] were used. The reference for one electron oxidation using this method was estimated to be 128.4 kcal/mol. Compared to the absolute redox potential of the Ru^{III}/Ru^{II} couple (1.40 + 4.281 V) [45], which corresponds to an electron affinity of 131.0 kcal/mol, an error of 1.6 kcal/mol

Table 2
Calculated redox potentials (in V vs SHE) for various redox couples.

Complex	Redox couple	Redox potential
Mn_4–L_6	Mn_4(II,III,III,III)/Mn_4(II,II,III,III)	0.70
	Mn_4(III,III,III,III)/Mn_4(II,III,III,III)	0.49
	Mn_4(III,III,III,IV)/Mn_4(III,III,III,III)	1.21
	Mn_4(III,III,IV,IV)/Mn_4(III,III,III,IV)	1.04
	Mn_4(III,IV,IV,IV)/Mn_4(III,III,IV,IV)	1.32
Mn_4–L_5	Mn_4(III,IV,IV,IV)/Mn_4(III,III,IV,IV)	2.35
Mn_4–L_5–$(H_2O)_3$	Mn_4(III,III,IV,IV)/Mn_4(III,III,III,IV)	0.97
	Mn_4(III,IV,IV,IV)/Mn_4(III,III,IV,IV)	1.04
	Mn_4(IV,IV,IV,IV)/Mn_4(III,IV,IV,IV)	1.56
	Mn_4-superoxide/Mn_4-peroxide	0.46

Please cite this article in press as: R.-Z. Liao, P.E.M. Siegbahn, Mechanism for O—O bond formation in a biomimetic tetranuclear manganese cluster – A density functional theory study, J. Photochem. Photobiol. B: Biol. (2014), http://dx.doi.org/10.1016/j.jphotobiol.2014.12.005

(0.069 V) is presented for each oxidation step. The same value of 128.4 kcal/mol can be obtained by using just the experimental total driving force of −51.1 kcal/mol and accurately calculated total energies for water and dioxygen, as reported in the studies of PSII [35]. It should be noted that the small difference between 128.4 and 131.0 kcal/mol does not say anything about the accuracy of the calculated redox potentials and p*K*a values of the catalyst.

3. Results and discussion

The present investigation starts from the lowest oxidation state (Mn_4(II,II,III,III)) proposed for the tetranuclear Mn complex with six phosphate ligands (**1**), the structure of which is shown in Fig. 1. The model for **1** consists of 162 atoms, and the total charge is 0. In **1**, two oxo groups bridge the four Mn ions, and two water molecules coordinate to Mn1 and Mn2, respectively. A spin population analysis (Table 1) shows that Mn1 and Mn2 are Mn^{II}, while Mn3 and Mn4 are Mn^{III}.

From **1**, four sequential PCET oxidations lead to the formation of **5**, which is proposed to initiate the O—O bond formation upon Mn—O charge transfer excitation at 337 nm [18]. In the transition from **1** to **2** (Fig. 2), Mn1 is oxidized from Mn^{II} to Mn^{III} (spin density of 3.96), and a proton is released from the water molecule that is ligated to Mn1. The redox potential for this transition was calculated to be 0.70 V (Table 2) vs the standard hydrogen electrode (SHE). Next, a PCET results in the formation of **3** (Mn_4(III,III,III,III)). During the oxidation, Mn2 is oxidized from Mn^{II} to Mn^{III} (spin density of 3.95), and a proton is released from the hydroxide that bridges Mn1, Mn2 and Mn4. The redox potential for this process was calculated to be only 0.49 V, which is 0.21 V lower than that

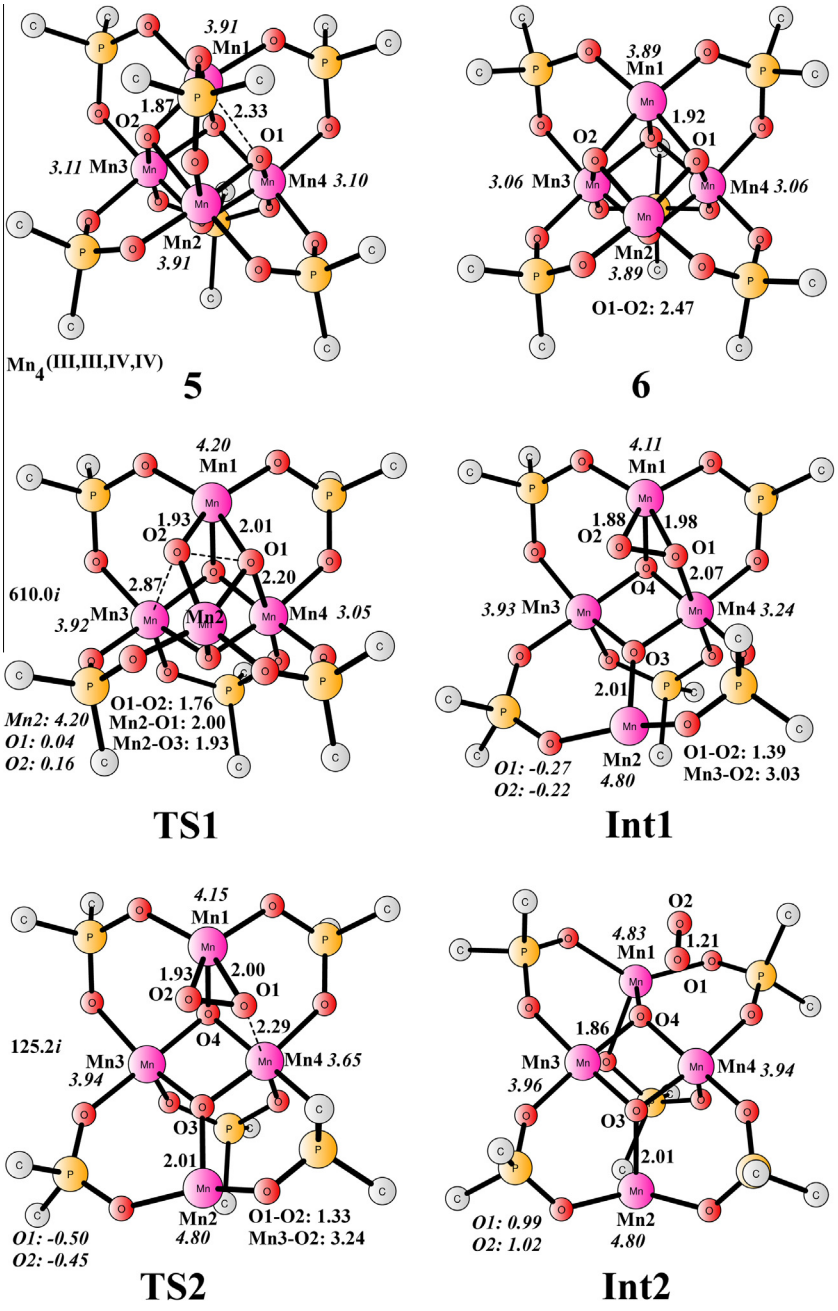

Fig. 3. Optimized structures for the O—O bond formation from **5**. Distances are given in Angstrom. Spin densities are shown in italic. The imaginary frequencies of **TS1** and **TS2** are indicated.

Please cite this article in press as: R.-Z. Liao, P.E.M. Siegbahn, Mechanism for O—O bond formation in a biomimetic tetranuclear manganese cluster – A density functional theory study, J. Photochem. Photobiol. B: Biol. (2014), http://dx.doi.org/10.1016/j.jphotobiol.2014.12.005

for the **2**/**1** couple. If the proton is released from the Mn1-bound water molecule, the redox potential would be 0.76 V, suggesting that this process is less favorable by 6.3 kcal/mol. This is followed by the transition of **3** to **4** (Mn_4(III,III,III,IV)), which is associated with a redox potential of 1.21 V. In this process, one electron is removed from Mn4 (spin density of 3.14) and one proton from the Mn2-bound water molecule. The transition from **4** to **5** has a calculated redox potential of 1.04 V. During the transition, one electron is removed from Mn3 coupled with the deprotonation of the hydroxide that bridges Mn1, Mn2 and Mn3. **5** can undergo phosphate dissociation upon excitation to generate **6** that has been proposed to enable the O—O bond formation in both gas phase and water solution. This process was calculated to be endergonic by 27.4 and 157.1 kcal/mol, respectively, in water solution and in gas phase, respectively. A difference of more than 10 kcal/mol can be seen between the present and the previous DFT calculations [29]. Two major reasons can be recognized. First, a simplified model was used in the previous study, in which the phenyl rings were represented by hydrogen atoms, while a full model is used here. Second, dispersion effect was considered in the present study while not before, which is known to be important for the modeling of the binding/dissociation of two molecules. Phosphate dissociation leads to a more compact structure of the tetranuclear core, as seen from the decrease of the Mn—Mn distances (Table 1). The O1—O2 distance decreases from 2.74 Å at **5** to 2.47 Å at **6**. In the previous investigation, the reason for this structural change was suggested to be due to the increased positive charge of **6** [29]. It should be pointed out that one electron oxidation of **5** is also possible leading to the formation of species **7** (Mn_4(III,IV,IV,IV)), with a calculated redox potential for this oxidation of 1.32 V. During the transition, Mn2 is oxidized from Mn^{III} to Mn^{IV} (spin density of 3.04). **7** was suggested to enable O_2 formation in a similar mechanism as **5**. Phosphate dissociation in **7** leads to the formation of **8**, and this process was calculated to be endergonic by 51.1 (199.3, gas phase value in parenthesis) kcal/mol. These values are much higher than that for **5** to **6**, due to the different total charge of **5** (0) and **7** (+1). Importantly, phosphate dissociation in **7** leads to a self oxidation reduction of the complex, where Mn2 is reduced from Mn^{IV} to Mn^{III}, and where the phosphate ligands are oxidized with one unpaired electron delocalized over the five phosphates. This is different from **5** to **6**, in which spin densities on Mn changes slightly upon phosphate dissociation. The oxidation of **6**–**8** has a redox potential of 2.35 V, which is significantly higher than that for the **7**/**5** transition.

Upon absorption of light, one phosphate ligand dissociates from **5** to generate species **6**, which can undergo O—O bond formation and O_2 release. The optimized transition states and intermediates are shown in Fig. 3. The potential energy profiles in the gas phase and in water solution are displayed in Fig. 4. In **6**, Mn1 and Mn2 are penta-coordinated with a vacant site on each metal. The direct coupling of the two bridging oxo groups O1 and O2 proceeds via **TS1** (Fig. 3) with a barrier of 42.3 kcal/mol in the gas phase. The barrier decreases to 28.5 kcal/mol by adding the water solvation effect. In **TS1**, the nascent O1—O2 bond distance is 1.76 Å, and O2 dissociates from Mn3 with a distance of 2.87 Å. **TS1** is characterized to be a transition state with an imaginary frequency of 610*i* cm^{-1}, which corresponds to the formation of the O1—O2 bond. From **6** to **TS1**, Mn3 becomes reduced from Mn^{IV} to Mn^{III} (spin density of 3.92), while from **TS1** to **Int1**, Mn2 dissociates from O1 and O2, and becomes reduced from Mn^{III} to Mn^{II} (spin density of 4.80). **Int1** lies at +8.9 (+31.1) kcal/mol relative to **6**. In **Int1**, the O1—O2 bond is formed coordinated to Mn1 in an η^2-fashion with a distance of 1.39 Å. The total spin density of this O_2 moiety is 0.47, suggesting a partial superoxide character. In the present work, the O—O bond formation and Mn2 dissociation take place in a concerted fashion, while a stepwise mechanism was suggested

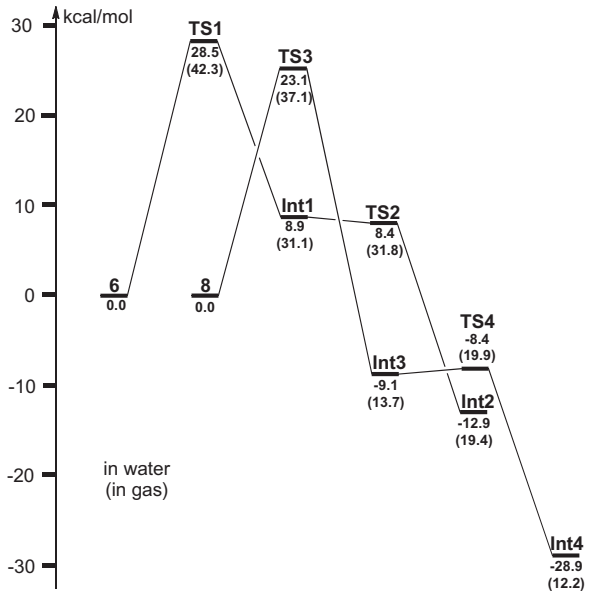

Fig. 4. Potential energy profile for the O—O bond formation from **6** and **8**, respectively.

in the previous study [29]. From **Int1**, O_2 dissociates from Mn4 and Mn1via **TS2**, which was calculated to be barrierless in solution. In **TS2**, the O1—O2 bond distance decreases to 1.33 Å, and a superoxide is formed with a total spin density of 0.95. Downhill from **TS2**, one electron is transferred from the O_2 moiety to Mn4, which becomes reduced to Mn^{III} (spin density of 3.94). The whole reaction from **6** to **Int2** is exergonic by 12.9 kcal/mol in solution, while it is endergonic by 19.4 kcal/mol in the gas phase. The very large solvation effect could be due to the large structural change during the reaction, as a more solvent accessible "open-butterfly" complex is formed in **Int2**.

Photoexcitation in gas phase clearly confirmed the formation of the O_2 molecule [18]. The barrier calculated in the gas phase is 42.3 kcal/mol in the ground state, which seems to be too high to overcome under normal conditions. However, it should be noted that the energy of light can be used to overcome this high barrier. Furthermore, the possibility of O—O bond formation in the excited state cannot be excluded.

To compare the relative reactivity of **6** and **8**, which have different oxidation states and total charges, **8** was also used as the starting structure for the O—O bond formation. The calculations show a similar O_2 formation mechanism as **6**. The whole reaction proceeds via two transition states, **TS3** and **TS4** (Fig. 5). The barrier for the first step was calculated to be 23.1 kcal/mol in solution, which is 5.4 kcal/mol lower than that from **6**. Similarly, the barrier in the gas phase is also about 5 kcal/mol lower, being 37.1 kcal/mol. This step (from **8** to **Int3**) is exergonic by 9.1 kcal/mol as compared with the endergonicity of 8.9 kcal/mol from **6** to **Int1**. During the O—O bond formation, one electron goes to the phosphate ligand radical and the other goes to Mn2, which is then reduced to Mn^{II} (spin density of 4.79). A major structural difference between **Int1** and **Int3** is that O2 is coordinated to Mn3 in **Int3** while it dissociates from Mn3 in **Int1**. O_2 release from **Int3** is associated with a very small barrier (0.7 kcal/mol) and the whole reaction is exergonic by 28.9 kcal/mol.

In the gas phase, the only choice for the O_2 evolution is to couple the two bridging oxygen atoms as discussed in the previous paragraph. In water solution, the solvent water molecules could affect the reaction by electrostatic interactions, which can be approximately captured by simply using a dielectric continuum

Please cite this article in press as: R.-Z. Liao, P.E.M. Siegbahn, Mechanism for O—O bond formation in a biomimetic tetranuclear manganese cluster – A density functional theory study, J. Photochem. Photobiol. B: Biol. (2014), http://dx.doi.org/10.1016/j.jphotobiol.2014.12.005

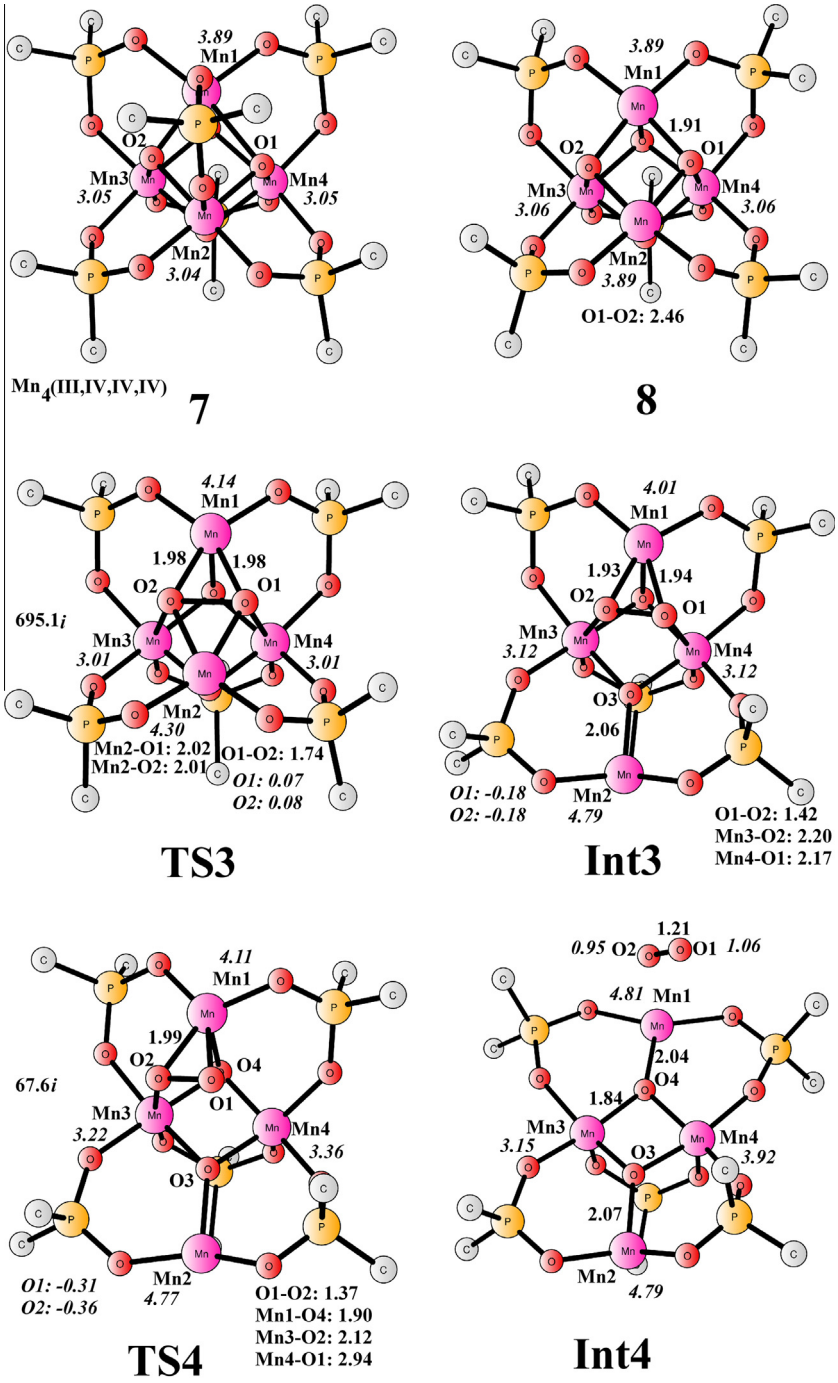

Fig. 5. Optimized structures for the O—O bond formation from **7**. Distances are given in Angstrom. Spin densities are shown in italic. The imaginary frequencies of **TS3** and **TS4** are indicated.

solvation model method. However, the other possibility is that the solvent water molecules can bind to Mn after phosphate release. This process is believed to be fast if there is enough driving force. In this case, the mechanism for the O—O bond formation could be different as the model is different from the gas phase one. Indeed, we found a different mechanism that has a lower barrier than the direct coupling mechanism as suggested for the gas phase. The proposed catalytic cycle starts from a Mn_4(III,III,III,IV) complex **9** that has a total charge of 0. **9** can be seen as derived from **4** by the dissociation of a phosphoric acid and the binding of three water molecules. In **9**, two water molecules bind to Mn1 and Mn2, respectively, and the third water molecule functions as a bridge and is hydrogen bonded to the two water molecules. Sequential PCET oxidations can generate **10** (Mn_4(III,III,IV,IV), Fig. 6) and **11** (Mn_4(III,IV,IV,IV)). The redox potentials for these two transitions were calculated to be 0.97 and 1.04 V, respectively. These values are lower than the reference redox potential 1.4 V, suggesting that both steps are exergonic (energy diagram see Fig. 7). From **9** to **10**, Mn4 is oxidized from Mn^{III} to Mn^{IV}, and from **10** to **11** Mn3 is oxidized from Mn^{III} to Mn^{IV}. In **10**, Mn1 is bound to a hydroxide ligand, and in **11** both Mn1 and Mn2 are bound to hydroxide ligands. The conversion of **6** (total charge of +1) to **10** (total charge of 0) by water binding and deprotonation has been calculated to be energetically very favorable. The binding of three water molecules to

Please cite this article in press as: R.-Z. Liao, P.E.M. Siegbahn, Mechanism for O—O bond formation in a biomimetic tetranuclear manganese cluster – A density functional theory study, J. Photochem. Photobiol. B: Biol. (2014), http://dx.doi.org/10.1016/j.jphotobiol.2014.12.005

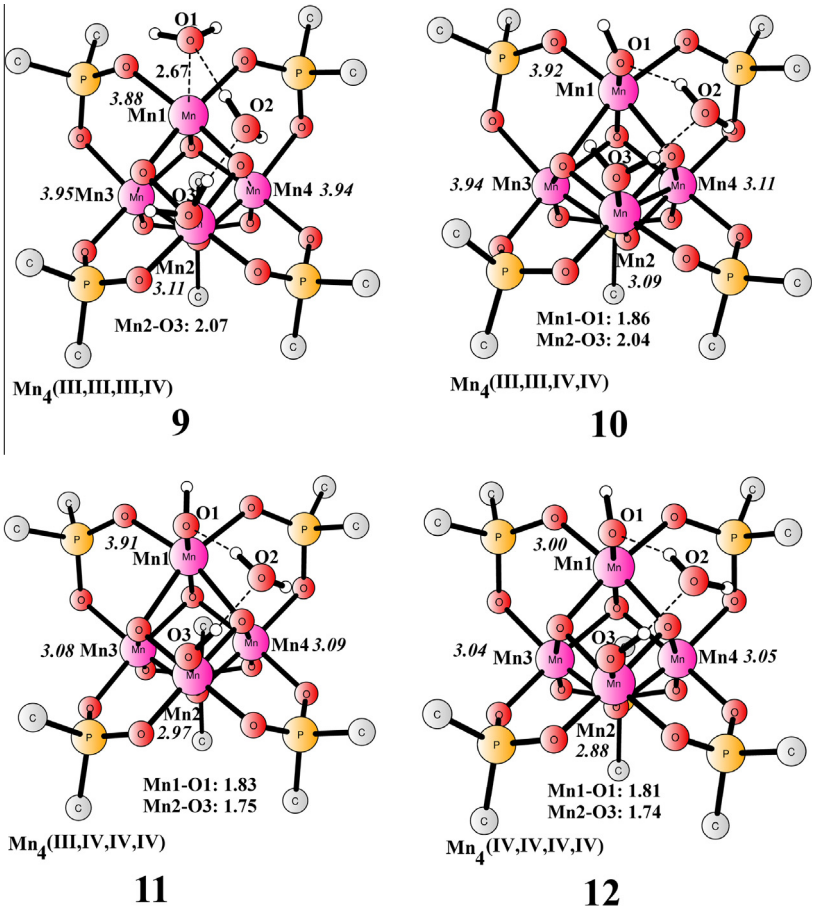

Fig. 6. Optimized structures of **9**, **10**, **11**, and **12**. Distances are given in Angstrom. Spin densities are shown in italic.

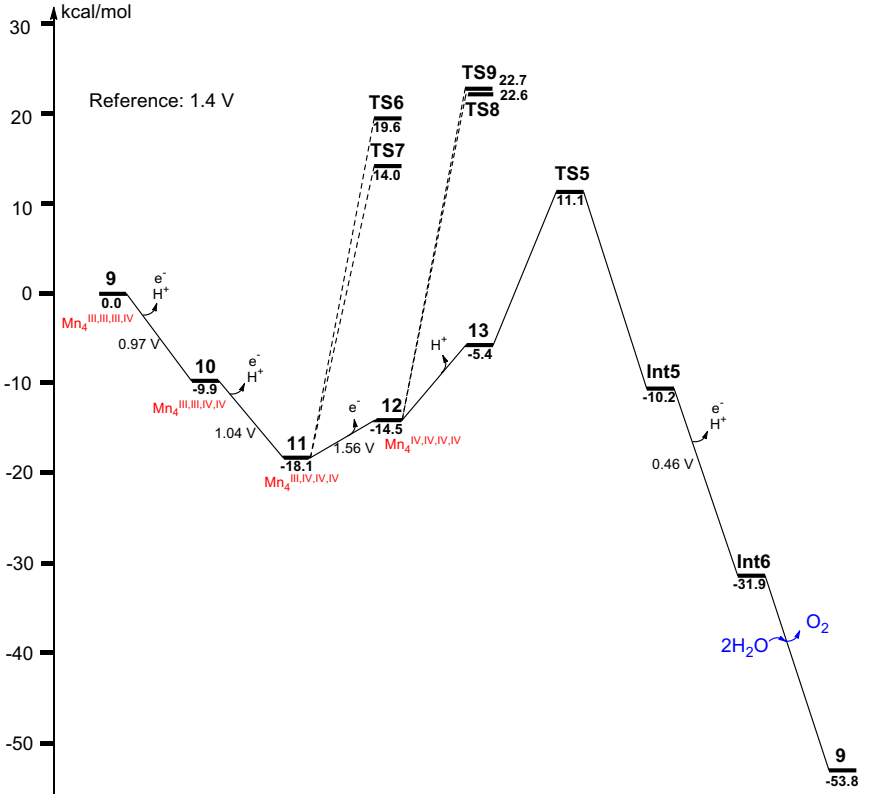

Fig. 7. Potential energy profile for the O—O bond formation from **9**, respectively.

Please cite this article in press as: R.-Z. Liao, P.E.M. Siegbahn, Mechanism for O—O bond formation in a biomimetic tetranuclear manganese cluster – A density functional theory study, J. Photochem. Photobiol. B: Biol. (2014), http://dx.doi.org/10.1016/j.jphotobiol.2014.12.005

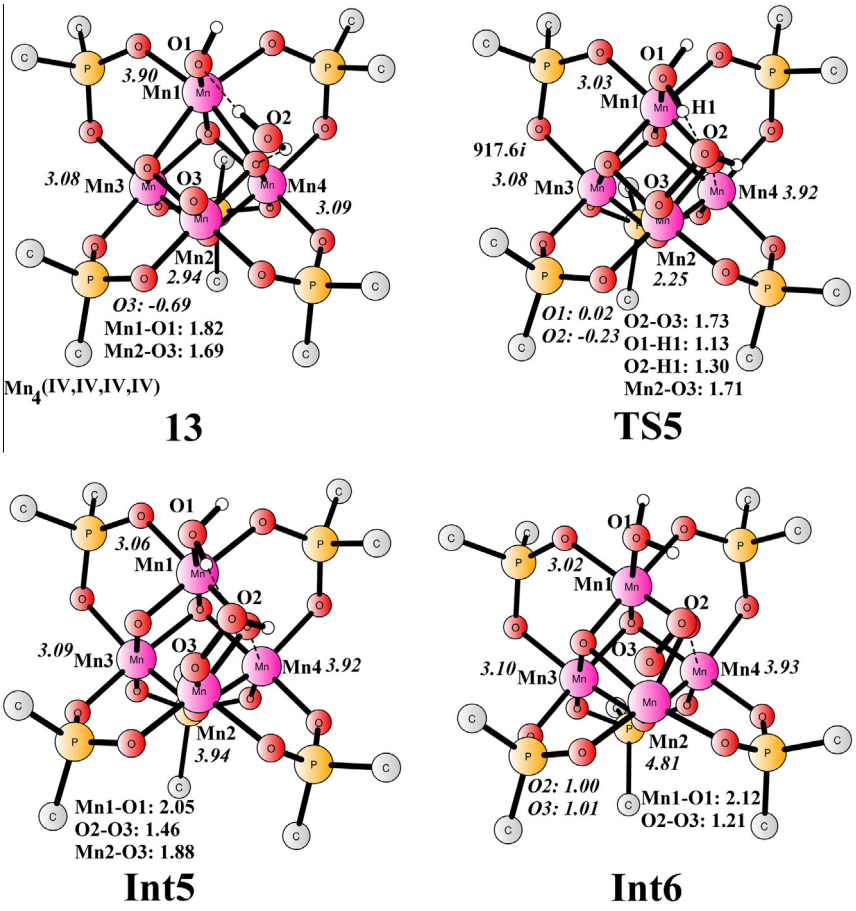

Fig. 8. Optimized structures for the O—O bond formation from **13**. Distances are given in Angstrom. Spin densities are shown in italic. The imaginary frequency of **TS5** is indicated.

6 was calculated to be exergonic by 12.7 kcal/mol. Since the p*K*a of this newly-formed species was calculated to be 4.7, under the working pH (6.5) this species becomes deprotonated to form **10** with an additional exergonicity of 2.5 kcal/mol. Similarly, the driving force for the conversion of **8** (total charge of +2) to **11** (total charge of 0) was also estimated. The water binding is exergonic by 25.9 kcal/mol, and further deprotonation ($pKa_1 = -5.2$ and $pKa_2 = 4.6$) to form a neutral complex is exergonic by 18.6 kcal/mol, resulting in a total exergonicity of more than 30 kcal/mol. In water solution, even though **8** is formed upon phosphate dissociation, its transformation to **11** is both thermodynamically and kinetically very facile.

The oxidation of **11** to form **12** (Mn_4(IV,IV,IV,IV)) turns out to be associated with the release of only one electron (redox potential of 1.56 V), rather than a PCET as for **9** and **10**. The p*K*a of **12** was calculated to be 13.2, and the deprotonation of **12** to form **13** (Fig. 8) at pH = 6.5 is thus endergonic by 9.1 kcal/mol. This deprotonation is coupled with intramolecular electron transfer from O3 to Mn1, consequently an oxyl radical is generated at O3 (spin density of −0.69) and Mn1 is reduced from Mn^{IV} to Mn^{III} (spin density of 3.90). In **13**, a Mn^{IV}-oxyl radical is formed and Mn2 is antiferromagnetically coupled with O3. The involvement of an Mn^{IV}-oxyl radical for the O—O bond formation has previously been suggested for photosystem II and a number of synthetic Mn complexes [46–50]. From **13**, the O—O bond formation can take place by a nucleophilic water attack on the Mn^{IV}-oxyl radical assisted by the Mn1-bound hydroxide, which functions as a base to abstract a proton during the attack. The optimized transition state **TS5** and the resulting intermediate **Int5** are shown in Fig. 8. The barrier was calculated to be 16.5 kcal/mol in 13-tet (19.7 kcal/mol in 15-tet) relative to **13**, and the total barrier is 29.2 kcal/mol relative to **11**. Compared with experimental kinetic data, which gave a barrier of about 20 kcal/mol, the calculated barrier seems to be overestimated. However, the energy of light can be used to overcome the high barrier, resulting in the lowering of the total barrier. Exactly how this happen is very difficult to model and is beyond the scope of the present study. In **TS5**, the distance between O2 and O3 is 1.73 Å, and the critical O2—H1 and O1—H1 distances are 1.30 and 1.13 Å, respectively. The electronic structure of Mn2—O3 changes from an Mn^{IV}-oxyl radical at **13** to Mn^{V} = O at **TS5**. In addition, one electron is transferred from Mn1 to Mn4 to accommodate the structural change during the attack. The resulting peroxide intermediate **Int5** lies at −4.8 kcal/mol relative to **13**. Since the high spin state of **Int5** is 15-tet, while it is 13-tet for **13**, a spin crossing is needed during the O—O bond formation. In **Int5**, Mn2 is reduced to Mn^{III}. Further PCET leads to O_2 formation and dissociation from Mn2 (**Int6**), which is coupled with the reduction of Mn2 from Mn^{III} to Mn^{II}. The redox potential for this transition was calculated to be 0.46 V. Finally, the exchange of O_2 by two water molecules can regenerate **9**, which is thermodynamically very feasible with an exergonicity of 21.9 kcal/mol.

The present mechanism is different from the leading suggestion for OEC in photosystem II, in which O—O bond formation takes place at the S_4 state (formally Mn_4(IV,IV,IV,V)) via the direct coupling of a Mn^{IV}-oxyl and a diMn bridging oxo with a calculated barrier of around 13 kcal/mol [48]. This is followed by O_2 release and the binding of a water molecule to start the next catalytic cycle. In the present case, the catalyst can only access the analogous S_3 state, Mn_4(IV,IV,IV,IV). In addition, in the present system, O—O bond formation proceeds via a nucleophilic water attack assisted

Please cite this article in press as: R.-Z. Liao, P.E.M. Siegbahn, Mechanism for O—O bond formation in a biomimetic tetranuclear manganese cluster – A density functional theory study, J. Photochem. Photobiol. B: Biol. (2014), http://dx.doi.org/10.1016/j.jphotobiol.2014.12.005

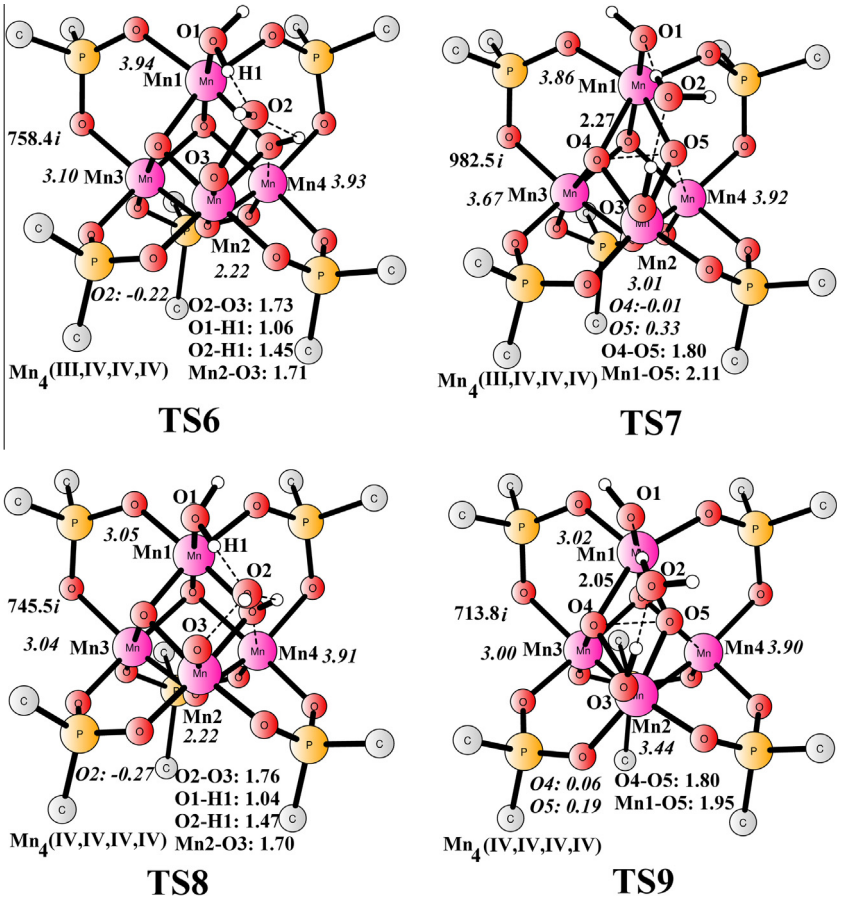

Fig. 9. Optimized transition state structures for the O—O bond formation from **11** to **12**. Distances are given in Angstrom. Spin densities are shown in italic. The imaginary frequencies of all transition states are indicated.

by a neighboring Mn–OH. An additional PCET has to take place to release O_2, which is different from that of the OEC. The different mechanism and the different oxidation states that lead to O—O bond formation may explain the different activity of the natural and the biomimetic catalysts. It should be pointed out that the degradation of the catalyst to form MnO_x nanoparticles has also been proposed as an alternative to rationalize the catalytic activity of $Mn_4O_4L_6$ immobilized on a Nafion membrane [51].

The O—O bond formation was also considered from **11** and **12** that have different oxidation states or protonation states compared with **13**. From **11**, two mechanistic scenarios can be envisioned, namely the water nucleophilic attack similar as **TS5** and the direct O—O coupling as **TS3**. For the water attack mechanism, a Mn^{IV}-oxyl radical has to be generated first by transferring the proton at the Mn2-bound hydroxide to one of the bridging oxo groups, which is coupled with electron transfer from O3 to Mn4. Then, the O—O bond formation proceeds via **TS6** (Mn_4(III,IV,IV,IV), Fig. 9) with a barrier of 37.7 kcal/mol relative to **11**. The barrier is thus 8.5 kcal/mol higher than that for **TS5** (Mn_4(IV,IV,IV,IV)). The alternative direct coupling of the bridging O4 and O5 (**TS7**) has a barrier of 32.1 kcal/mol, which is 9.0 kcal/mol higher than that from **8** (**TS3**, with water solvation effects considered by the continuum solvation model method), in which no hydroxide is bound to Mn1 or Mn2. Since the binding of water molecules to Mn1 and Mn2 takes place very easily in water solution, the mechanism for the O—O bond formation in the gas phase and in water solution is different. In addition, the barrier is still 2.9 kcal/mol higher than the water attack mechanism via **TS5**, suggesting O—O bond formation at the higher oxidation state Mn_4(IV,IV,IV,IV). The O—O bond formation from **12** can take place via **TS8** and **TS9** (Fig. 9), the barriers of which were calculated to be 40.7 and 40.8 kcal/mol relative to **11**, respectively. These values are much higher than that from **13** even though an energy penalty of 9.1 kcal/mol has to be paid for the removal of a proton from **12**.

4. Conclusions

In the present paper, the reaction mechanism for water oxidation catalyzed by a tetranuclear Mn-oxo cluster $Mn_4O_4L_6$ ($L = (C_6H_4)_2PO_4^-$) was studied. The reaction mechanism of the O—O bond formation was found to be different in gas phase and in water solution.

The experimentally suggested mechanism was first investigated, in which the reaction starts from Mn_4(II,II,III,III)-L_6 with two bridging oxo groups and two weakly-coordinated water molecules. Four sequential PCET oxidations lead to the formation of Mn_4(III,III,IV,IV)-L_6 (**5**) with four bridging oxo groups. A further one electron oxidation can generate a Mn_4(III,IV,IV,IV)-L_6 (**7**) species. In gas phase, upon illumination, both **5** and **7** undergo the dissociation of one phosphate ligand. This is followed by the direct coupling of two bridging oxo groups, which was calculated to be rate-limiting with a very high barrier (around 40 kcal/mol). The following O_2 release step was found to be very easy and the reaction is endergonic by more than 10 kcal/mol. In the ground state, the O—O bond formation is thus thermodynamically and kinetically very unfavorable. However, the energy of light can be used to overcome this high barrier and the possibility of involving excited states for the O—O bond formation cannot be ruled out.

In aqueous solution, the dissociation of phosphate results in two vacant metal coordination sites, and the ligation of water

Please cite this article in press as: R.-Z. Liao, P.E.M. Siegbahn, Mechanism for O—O bond formation in a biomimetic tetranuclear manganese cluster – A density functional theory study, J. Photochem. Photobiol. B: Biol. (2014), http://dx.doi.org/10.1016/j.jphotobiol.2014.12.005

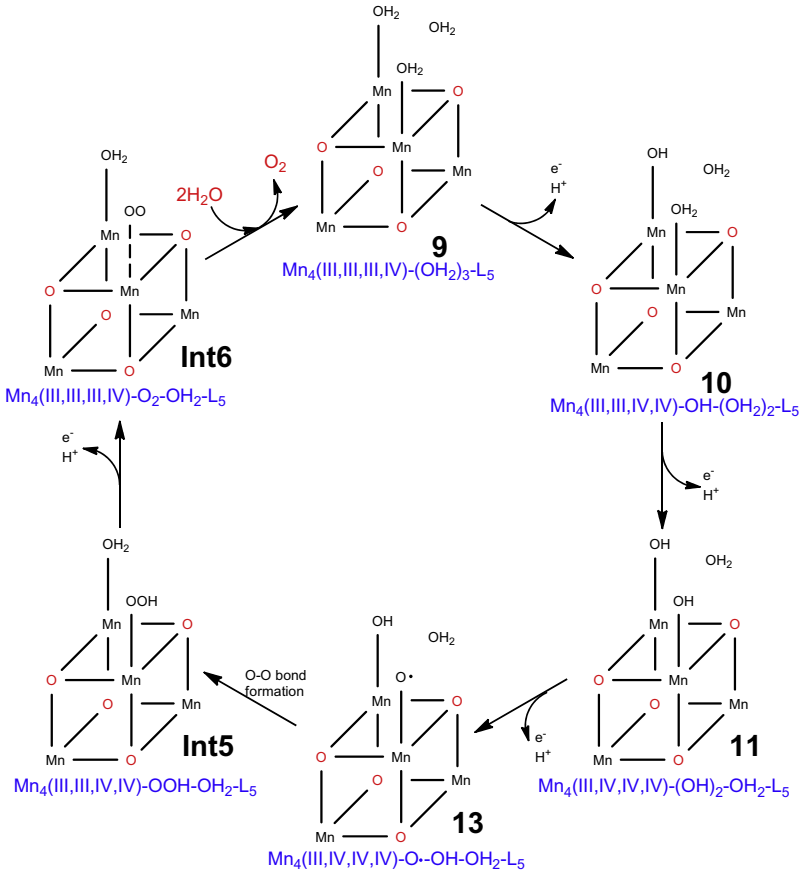

Scheme 2. Proposed catalytic cycle for water oxidation catalyzed by $Mn_4O_4L_6$ in water solution.

molecules was found to be highly exergonic. The catalytic species is thus different from the one in the gas phase. The reaction starts from Mn_4(III,III,III,IV)-L_5 (**9**) with three water molecules, in which two of them are ligands to two Mn ions (Scheme 2). Two PCET oxidations lead to the generation of a Mn_4(III,IV,IV,IV) species (**11**), and the redox potentials of both steps are around 1.0 V. One electron oxidation of **11** to produce **12** (Mn_4(IV,IV,IV,IV)) has a redox potential of 1.56 V, which is higher than the reference redox potential (1.40 V). These results suggest that **11** is the resting state for the whole catalytic cycle. The deprotonation of **12** can form an Mn^{IV}-oxyl radical (**13**), which undergoes a water nucleophilic attack facilitated by a Mn-bound hydroxide. The barrier for the O—O bond formation by water attack was calculated to be 16.5 kcal/mol relative to **13**, and the total barrier became 29.2 kcal/mol when the energy penalty for the formation of **13** was added. A further PCET transition leads to the dissociation of the O_2 molecule, and the exchange of O_2 by two water molecules can regenerate **9** for the next catalytic cycle. The calculated barrier of 29.2 kcal/mol is much higher than the one derived from the experimental kinetic study (about 20 kcal/mol). It is therefore suggested here that, similarly to the case in gas phase, the energy of light can be used to overcome this high barrier and accelerate the reaction.

Acknowledgments

We acknowledge the Swedish Research Council and the Knut and Alice Wallenberg Foundation for financial support. Computer time was generously provided by the Swedish National Infrastructure for Computing.

Appendix A. Supplementary material

Supplementary data associated with this article can be found, in the online version, at http://dx.doi.org/10.1016/j.jphotobiol.2014.12.005.

References

[1] K.N. Ferreira, T.M. Iverson, K. Maghlaoui, J. Barber, S. Iwata, Architecture of the photosynthetic oxygen-evolving center, Science 303 (2004) 1831–1838.
[2] B. Loll, J. Kern, W. Saenger, A. Zouni, J. Biesiadka, Towards complete cofactor arrangement in the 3.0 Å resolution structure of photosystem II, Nature 438 (2005) 1040–1044.
[3] A. Guskov, J. Kern, A. Gabdulkhakov, M. Broser, A. Zouni, W.J. Saenger, Cyanobacterial photosystem II at 2.9-Å resolution and the role of quinones, lipids, channels and chloride, Nat. Struct. Mol. Biol. 16 (2009) 334–341.
[4] Y. Umena, K. Kawakami, J.-R. Shen, N. Kamiya, Crystal structure of oxygen-evolving photosystem II at a resolution of 1.9 Å, Nature 473 (2011) 55–60.
[5] J. Limburg, J.S. Vrettos, L.M. Liable-Sands, A.L. Rheingold, R.H. Crabtree, G.W. Brudvig, A functional model for O–O bond formation by the O_2-evolving complex in photosystem II, Science 283 (1999) 1524–1527.
[6] Y. Shimazaki, T. Nagano, H. Takesue, B.-H. Ye, F. Tani, Y. Naruta, Characterization of a dinuclear Mn^V = O complex and its efficient evolution of O2 in the presence of water, Angew. Chem. Int. Ed. 43 (2004) 98–100.
[7] M. Yagi, K. Narita, Catalytic O_2 evolution from water induced by adsorption of $[(OH_2)(Terpy)Mn(\mu\text{-}O)_2Mn(Terpy)(OH_2)]^{3+}$ complex onto clay compounds, J. Am. Chem. Soc. 126 (2004) 8084–8085.
[8] A.K. Poulsen, A. Rompel, C.J. McKenzie, Water oxidation catalyzed by a dinuclear Mn complex: a functional model for the oxygen-evolving center of photosystem II, Angew. Chem. Int. Ed. 44 (2005) 6916–6920.
[9] K. Beckmann, H. Uchtenhagen, G. Berggren, M.F. Anderlund, A. Thapper, J. Messinger, S. Styring, P. Kurz, Formation of stoichiometrically ^{18}O-labelled oxygen from the oxidation of ^{18}O-enriched water mediated by a dinuclear manganese complex – a mass spectrometry and EPR study, Energy Environ. Sci. 1 (2008) 668–676.
[10] Y. Gao, T. Åkermark, J. Liu, L. Sun, B. Åkermark, Nucleophilic attack of hydroxide on a Mn^V oxo complex: a model of the O–O bond formation in the

oxygen evolving complex of photosystem II, J. Am. Chem. Soc. 131 (2009) 8726–8727.
[11] E.A. Karlsson, B.-L. Lee, T. Åkermark, E.V. Johnston, M.D. Kärkäs, J. Sun, Ö. Hansson, J.-E. Bäckvall, B. Åkermark, Photosensitized water oxidation by use of a bioinspired manganese catalyst, Angew. Chem. Int. Ed. 50 (2011) 11715–11718.
[12] J.S. Kanady, E.Y. Tsui, M.W. Day, T. Agapie, A synthetic model of the Mn_3Ca subsite of the oxygen-evolving complex in photosystem II, Science 333 (2011) 733–736.
[13] H.-M. Berends, A.-M. Manke, C. Näther, F. Tuczek, P. Kurz, A manganese oxido complex bearing facially coordinating trispyridyl ligands – is coordination geometry crucial for water oxidation catalysis?, Dalton Trans 41 (2012) 6215–6224.
[14] K.J. Young, M.K. Takase, G.W. Brudvig, An anionic N-donor ligand promotes manganese-catalyzed water oxidation, Inorg. Chem. 52 (2013) 7615–7622.
[15] G.C. Dismukes, R. Brimblecombe, G.A.N. Felton, R.S. Pryadun, J.E. Sheats, L. Spiccia, G.F. Swiegers, Development of bioinspired Mn_4O_4-cubane water oxidation catalysis: lessons from photosynthesis, Acc. Chem. Res. 42 (2009) 1935–1943.
[16] W.F. Ruettinger, C. Campana, G.C. Dismukes, Synthesis and characterization of $Mn_4O_4L_6$ complexes with cubane-like core structure: a new class of models of the active site of the photosynthetic water oxidase, J. Am. Chem. Soc. 119 (1997) 6670–6671.
[17] W.F. Ruettinger, D.M. Ho, G.C. Dismukes, Protonation and dehydration reactions of the $Mn_4O_4L_6$ cubane and synthesis and crystal structure of the oxidized cubane $[Mn_4O_4L_6]^+$: a model for the photosynthetic water oxidizing complex, Inorg. Chem. 38 (1999) 1036–1037.
[18] W.F. Ruettinger, G.C. Dismukes, Conversion of core oxos to water molecules by $4e^-/4H^+$ reductive dehydration of the $Mn_4O_2^{6+}$ core in the manganese-oxo cubane complex $Mn_4O_4(Ph_2PO_2)_6$: a partial model for photosynthetic water binding and activation, Inorg. Chem. 39 (2000) 1021–1027.
[19] W.F. Ruettinger, M. Yagi, W.S. Bernasek, G.C. Dismukes, O_2 evolution from the manganese-oxo cubane core $Mn_4O_4^{6+}$: a molecular mimic of the photosynthetic water oxidation enzyme?, J Am. Chem. Soc. 122 (2000) 10353–10357.
[20] M. Yagi, K.V. Wolf, P.J. Baesjou, S.L. Bernasek, G.C. Dismukes, Selective photoproduction of O_2 from the Mn_4O_4 cubane core: a structural and functional model for the photosynthetic water-oxidizing complex, Angew. Chem. Int. Ed. 40 (2001) 2925–2928.
[21] M. Maneiro, W.F. Ruettinger, E. Bourles, G.L. McLendon, G.C. Dismukes, Kinetics of proton-coupled electron-transfer reactions to the manganese-oxo "cubane" complexes containing the $Mn_4O_4^{6+}$ and $Mn_4O_4^{7+}$ core types, Proc. Natl. Acad. Sci. USA 100 (2003) 3707–3712.
[22] T.G. Carrell, E. Bourles, M. Lin, G.C. Dismukes, Transition from hydrogen atom to hydride abstraction by $Mn_4O_4(O_2PPh_2)_6$ versus $[Mn_4O_4(O_2PPh_2)_6]^+$: O–H bond dissociation energies and the formation of $Mn_4O_3(OH)(O_2PPh_2)_6$, Inorg. Chem. 42 (2003) 2849–2858.
[23] J.-Z. Wu, E. Sellitto, G.P.A. Yap, J. Sheats, G.C. Dismukes, Trapping an elusive intermediate in manganese-oxo cubane chemistry, Inorg. Chem. 43 (2004) 5795–5797.
[24] J.-Z. Wu, F. De Angelis, T.G. Carrell, G.P.A. Yap, J. Sheats, R. Car, G.C. Dismukes, Tuning the photoinduced O_2-evolving reactivity of $Mn_4O_4^{7+}$, $Mn_4O_4^{6+}$, $Mn_4O_3(OH)^{6+}$ mamnanese-oxo cubane complexes, Inorg. Chem. 45 (2006) 189–195.
[25] R. Brimblecombe, G.F. Swiegers, G.C. Dismukes, L. Spiccia, Substained water oxidation photocatalysis by a bioinspired manganese cluster, Angew. Chem. Int. Ed. 47 (2008) 7335–7338.
[26] R. Brimblecombe, A.M. Bond, G.C. Dismukes, G.F. Swiegers, L. Spiccia, Electrochemical investigation of Mn_4O_4-cubane water-oxidizing clusters, Phys. Chem. Chem. Phys. 11 (2009) 6441–6449.
[27] R. Brimblecombe, D.R.J. Kolling, A.M. Bond, G.C. Dismukes, G.F. Swiegers, L. Spiccia, Substained water oxidation by $[Mn_4O_4]^{7+}$ core complexes inspired by oxygenic photosynthesis, Inorg. Chem. 48 (2009) 7269–7279.
[28] R. Brimblecombe, A. Koo, G.C. Dismukes, G.F. Swiegers, L. Spiccia, Solar driven water oxidation by a bioinspired manganese molecular catalyst, J. Am. Chem. Soc. 132 (2010) 2892–2894.
[29] A.E. Kuznetsov, Y.V. Geletii, C.L. Hill, D.G. Musaev, Insights into the mechanism of O_2 formation and release from the $Mn_4O_4L_6$ "cubane" cluster, J. Phys. Chem. A 114 (2010) 11417–11424.
[30] P.E.M. Siegbahn, A structure-consistent mechanism for dioxygen formation in photosystem II, Chem. Eur. J. 14 (2008) 8290–8302.
[31] P.E.M. Siegbahn, M.R.A. Blomberg, Quantum chemical studies of proton-coupled electron transfer in metalloenzymes, Chem. Rev. 110 (2010) 7040–7061.
[32] X. Li, G. Chen, S. Schinzel, P.E.M. Siegbahn, A comparison between artificial and natural water oxidation, Dalton. Trans. 40 (2011) 11296–11307.
[33] P.E.M. Siegbahn, Recent theoretical studies of water oxidation in photosystem II, J. Photochem. Photobiol. B 104 (2011) 94–99.
[34] X. Li, P.E.M. Siegbahn, Water oxidation mechanism for synthetic Co-oxides with small nuclearity, J. Am. Chem. Soc. 135 (2013) 13804–13813.
[35] P.E.M. Siegbahn, M.R.A. Blomberg, Energy diagrams for water oxidation in photosystem II using different density functionals, J. Chem. Theory Comput. 10 (2014) 268–272.
[36] R.Z. Liao, X. Li, P.E.M. Siegbahn, Reaction mechanism of water oxidation catalyzed by iron tetraamido macrocyclic ligand complexes – A DFT study, Eur. J. Inorg. Chem. (2014) 728–741.
[37] R.Z. Liao, P.E.M. Siegbahn, Which oxidation state leads to O–O bond formation in Cp*Ir(bpy)Cl-catalyzed water oxidation, Ir(V). Ir(VI), or Ir(VII)?, ACS Catal 4 (2014) 3937–3949.
[38] A.D. Becke, Density-functional thermochemistry. III. The role of exact exchange, J. Chem. Phys. 98 (1993) 5648–5652.
[39] M.J. Frisch, G.W. Trucks, H.B. Schlegel, G.E. Scuseria, M.A. Robb, J.R. Cheeseman, G. Scalmani, V. Barone, B. Mennucci, G.A. Petersson, et al., Gaussian 09, Revision C.01, Gaussian Inc, Wallingford CT, 2009.
[40] M. Dolg, U. Wedig, H. Stoll, H. Preuss, Energy-adjusted ab initio pseudopotentials for the first row transition elements, J. Chem. Phys. 86 (1987) 866–872.
[41] M. Reiher, O. Salomon, B.A. Hess, Reparameterization of hybrid functionals based on energy differences of states of different multiplicity, Theor. Chem. Acc. 107 (2001) 48–55.
[42] A.V. Marenich, C.J. Cramer, D.G. Truhlar, Universal solvation model based on solute electron density and on a continuum model of the solvent defined by the bulk dielectric constant and atomic surface tensions, J. Phys. Chem. B 113 (2009) 6378–6396.
[43] D.M. Camaioni, C.A. Schwerdtfeger, Comment on Accurate experimental values for the free energies of hydration of H^+, OH^-, and H_3O^+, J. Phys. Chem. A 109 (2005) 10795–10797.
[44] S. Grimme, Semiempirical GGA-type density functional constructed with a long-range dispersion correction, J. Comput. Chem. 27 (2006) 1787–1799.
[45] A.A. Isse, A. Gennaro, Absolute potential of the standard hydrogen electrode and the problem of interconversion of potentials in different solvents, J. Phys. Chem. B 114 (2010) 7894–7899.
[46] P.E.M. Siegbahn, O–O bond formation in the S_4 state of the oxygen-evolving complex in photosystem II, Chem. Eur. J. 12 (2006) 9217–9227.
[47] P.E.M. Siegbahn, Structures and energetics for O_2 formation in photosystem II, Acc. Chem. Res. 42 (2009) 1871–1880.
[48] P.E.M. Siegbahn, Water oxidation mechanism in photosystem II, including oxidations, proton release pathways, O–O bond formation and O_2 release, Biochim. Biophys. Acta 2013 (1827) 1003–1019.
[49] M. Lundberg, M.R.A. Blomberg, P.E.M. Siegbahn, Oxyl radical required for O–O bond formation in synthetic Mn-catalyst, Inorg. Chem. 43 (2004) 264–274.
[50] W.M.C. Sameera, C.J. McKenzie, J.E. McGrady, On the mechanism of water oxidation by a bimetallic manganese catalyst: a density functional study, Dalton Trans. 40 (2011) 3859–3870.
[51] R.K. Hocking, R. Brimblecombe, L.-Y. Chang, A. Singh, M.H. Cheah, C. Glover, W.H. Casey, L. Spiccia, Water-oxidation catalysis by manganese in a geochemical-like cycle, Nat. Chem. 3 (2011) 461–466.

Please cite this article in press as: R.-Z. Liao, P.E.M. Siegbahn, Mechanism for O—O bond formation in a biomimetic tetranuclear manganese cluster – A density functional theory study, J. Photochem. Photobiol. B: Biol. (2014), http://dx.doi.org/10.1016/j.jphotobiol.2014.12.005